

Mean Value Coordinates for Arbitrary Planar Polygons

KAI HORMANN

Clausthal University of Technology

and

MICHAEL S. FLOATER

University of Oslo

Barycentric coordinates for triangles are commonly used in computer graphics, geometric modeling, and other computational sciences because they provide a convenient way to linearly interpolate the data that is given at the corners of a triangle. The concept of barycentric coordinates can also be extended in several ways to convex polygons with more than three vertices, but most of these constructions break down when used in the nonconvex setting. *Mean value coordinates* offer a choice that is not limited to convex configurations, and we show that they are in fact well-defined for arbitrary planar polygons without self-intersections. Besides their many other important properties, these coordinate functions are smooth and allow an efficient and robust implementation. They are particularly useful for interpolating data that is given at the vertices of the polygons and we present several examples of their application to common problems in computer graphics and geometric modeling.

Categories and Subject Descriptors: G.1.1 [Numerical Analysis]: Interpolation—*Interpolation formulas*; I.3.3 [Computer Graphics]: Picture/Image Generation; J.6 [Computer Applications]: Computer-Aided Engineering—*Computer-aided design (CAD)*; I.3.7 [Computer Graphics]: Three-Dimensional Graphics and Realism—*Color, shading, shadowing, and texture*

General Terms: Algorithms, Theory

Additional Key Words and Phrases: Barycentric coordinates, interpolation

1. INTRODUCTION

It follows from Ceva's Theorem [Ceva 1678] that for any point v inside a planar triangle $[v_1, v_2, v_3]$, there exist three masses w_1 , w_2 , and w_3 , such that if placed at corresponding vertices of the triangle, their center of mass (or barycenter) will coincide with v , that is,

$$\frac{w_1 v_1 + w_2 v_2 + w_3 v_3}{w_1 + w_2 + w_3} = v. \quad (1)$$

Möbius [1827] was the first to study such *mass points* and he defined w_1 , w_2 , and w_3 as the *barycentric coordinates* of v . Evidently, these barycentric coordinates are only unique up to multiplication by a common nonzero scalar and they are usually *normalized* to sum to one.

These normalized triangular barycentric coordinates are linear in v and have the additional property that the i -th coordinate has value 1 at v_i and 0 at the other v_j . This is why they are commonly used

Authors' addresses: K. Hormann, Department of Informatics, Clausthal University of Technology, Julius-Albert-Str. 4, 38678 Clausthal-Zellerfeld, Germany; email: kai.hormann@tu-clausthal.de; M. S. Floater, Department of Informatics, University of Oslo, P.O. Box 1053 Blindern, 0316 Oslo, Norway; email: michael@ifi.uio.no.

Permission to make digital or hard copies of part or all of this work for personal or classroom use is granted without fee provided that copies are not made or distributed for profit or direct commercial advantage and that copies show this notice on the first page or initial screen of a display along with the full citation. Copyrights for components of this work owned by others than ACM must be honored. Abstracting with credit is permitted. To copy otherwise, to republish, to post on servers, to redistribute to lists, or to use any component of this work in other works requires prior specific permission and/or a fee. Permissions may be requested from Publications Dept., ACM, Inc., 2 Penn Plaza, Suite 701, New York, NY 10121-0701 USA, fax +1 (212) 869-0481, or permissions@acm.org.

© 2006 ACM 0730-0301/06/1000-1424 \$5.00

ACM Transactions on Graphics, Vol. 25, No. 4, October 2006, Pages 1424–1441.

to linearly interpolate the values given at the vertices of a triangle and have applications in computer graphics (e.g., Gouraud and Phong shading, texture mapping, ray-triangle intersection), geometric modeling (e.g., triangular Bézier patches, splines over triangulations), and many other fields (e.g., the finite element method, terrain modeling).

In many applications it would be useful to have a generalization of barycentric coordinates to arbitrary n -sided polygons, or even sets of polygons in the plane with vertices v_1, \dots, v_n . We would then like to have smooth *homogeneous barycentric coordinates* $w_i : \mathbb{R}^2 \rightarrow \mathbb{R}$ that generalize Eq. (1),

$$\sum_{i=1}^n w_i(v)(v_i - v) = 0, \quad (2)$$

and associated *normalized barycentric coordinates*,

$$\lambda_i(v) = \frac{w_i(v)}{\sum_{j=1}^n w_j(v)}, \quad (3)$$

so that any point v in the plane can be written as an *affine combination* of v_1, \dots, v_n with weights $\lambda_1(v), \dots, \lambda_n(v)$. Furthermore, these coordinates should satisfy the Lagrange property

$$\lambda_i(v_j) = \delta_{i,j} = \begin{cases} 1 & \text{if } i = j, \\ 0 & \text{if } i \neq j. \end{cases} \quad (4)$$

We discuss a general approach to constructing such homogeneous barycentric coordinates in Section 3, but for most choices, the normalized coordinates in Eq. (3) either are not well-defined everywhere in \mathbb{R}^2 or do not meet the constraints in Eq. (4). We then prove in Section 4 that *mean value coordinates* fulfill both conditions and have a number of other important properties, such as smoothness, linear independence, and refinability. They further enable a very efficient and robust implementation, as shown in Section 5.

The main application of these coordinates is interpolation, and in Section 6 we give several examples from computer graphics and geometric modeling that can be seen as interpolation problems and hence solved with this approach. In particular, we propose an improved Phong shading method for nontriangular faces, a simple image warping technique, and interpolation of data that is specified on planar curves.

2. RELATED WORK

2.1 Barycentric Coordinates

Most previous work on barycentric coordinates discusses the extension to *convex* polygons. The first such generalization appears in the pioneering work of Wachspress [1975], who was interested in extending the finite element method. These *Wachspress coordinates* are rational polynomials and were later generalized to convex polytopes by Warren [1996], who also showed that they have minimal degree [Warren 2003]. They can be computed with simple and local formulae in the plane [Meyer et al. 2002], as well as in higher dimensions [Warren et al. 2004], and have many other nice properties like affine invariance. A simple geometric construction has recently been presented by Ju et al. [2005]. Malsch and Dasgupta have also been interested in finite element methods and extended Wachspress' approach to weakly convex polygons [Malsch and Dasgupta 2004a] and convex polygons with interior nodes [Malsch and Dasgupta 2004b].

Other generalizations of barycentric coordinates to convex polygons, and even to the kernel of a star-shaped polygon, were presented in the context of triangle mesh parameterization, for example, *shape preserving* [Floater 1997], *discrete harmonic* [Pinkall and Polthier 1993; Eck et al. 1995], and mean

value coordinates [Floater 2003]. The latter have also been generalized to polyhedra of arbitrary genus in 3D independently by Floater et al. [2005] and Ju et al. [2005].

Also, the *natural neighbor interpolants* that were proposed by Sibson [1980, 1981] for the purpose of scattered data interpolation provide barycentric coordinates for convex polygons, but like the coordinates in Farin [1990], they are not more than C^1 -continuous away from the data points. Hiyoshi and Sugihara [2000] extended Sibson's approach and presented C^k -continuous coordinates, but their computation is very costly and involves numerical integration.

Except for discrete harmonic coordinates, all these coordinates have in common that they are *positive* over the interior of any convex polygon. In fact, this property has often been used in the definition of barycentric coordinates, instead of the weaker interpolation condition of Eq. (4), which is in any case a consequence of the positivity, as discussed by Floater et al. [2006]. They also proved that for a convex polygon, the Wachspress and mean value coordinates are the only positive coordinates with uniform scaling invariance that can be computed with a local three-point formula.

For *nonconvex* polygons, a usual approach is to triangulate the domain and apply the standard barycentric coordinates on each triangle, but the result depends on the particular triangulation chosen and is only C^0 -continuous over the edges of the triangles. To the best of our knowledge, Malsch and Dasgupta [2005] were the first to present smooth barycentric coordinates for nonconvex polygons. Their coordinate functions are well-defined over the *convex hull* of any concave polygon with possible holes, and the construction requires special treatment of the vertices on the convex hull. Based on the work of Malsch et al. [2005], Sukumar and Malsch [2006] recently suggested another type of smooth barycentric coordinates for nonconvex polygons that are not restricted to the convex hull, but these *metric coordinates* are no longer necessarily positive over the interior of a convex polygon.

Contributions. We show that the mean value coordinates can also be used in the nonconvex setting and even more generally, for sets of arbitrary planar polygons without self-intersections. In particular, they are well-defined everywhere in the plane and can be computed with a simple and local formula. These properties make them an ideal tool for the interpolation of data that is given at the vertices. We also show that the mean value coordinates are smooth (i.e., C^∞), except at the vertices of the input polygons (where they are only C^0 -continuous).

2.2 Interpolation

The interpolation of data that is given at the vertices of a set of polygons can be seen as a scattered data interpolation (SDI) problem and many different approaches exist to solve it, including radial basis functions [Beatson and Newsam 1992; Beatson et al. 2000; Buhmann 2000] and bivariate splines [Lee et al. 1997; Nürnberger and Zeilfelder 2000]. Such interpolation problems frequently occur in various fields of science and engineering (e.g., geology, reverse engineering, numerical simulation), but also in computer graphics and geometric modeling.

For example, *image warping* (see Wolberg [1990], Glasbey and Mardia [1998], and Milliron et al. [2002] for an overview of the state-of-the-art) can be seen as an interpolation problem, and radial basis functions [Arad et al. 1994; Ruprecht and Müller 1995] as well as B-splines [Lee et al. 1995, 1997] have been used to solve it.

Another important problem is that of *transfinite interpolation*, where the data to be interpolated is given as functions over a set or network of planar curves. There exist a number of well-established methods for some special cases, such as Coons' or Gordon surfaces [Farin 2002] for triangular- or rectangular-shaped input curves, but very few are known for the general case. The standard approach is to either sample the data and apply an SDI method or to solve a partial differential equation (PDE) with the given data as boundary conditions [Chai et al. 1998; Kounchev 2001]. But like the generalization of Sibson's interpolants that was suggested by Gross and Farin [1999], this is usually very costly to compute.

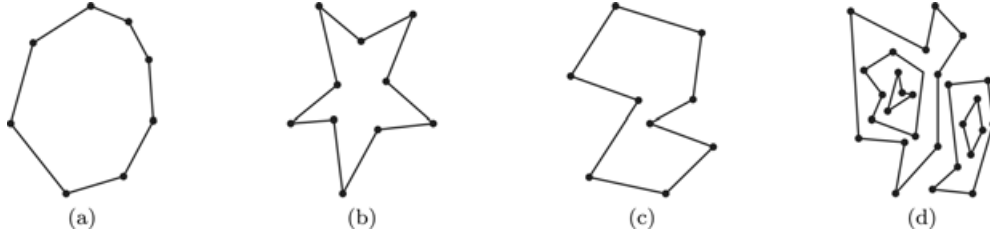


Fig. 1. We consider (a) convex, (b) star-shaped, (c) simple, and (d) sets of simple polygons.

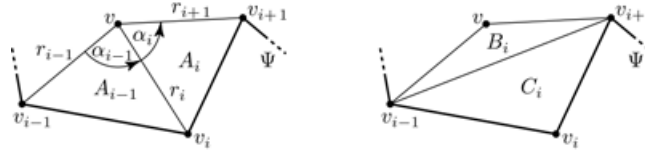


Fig. 2. Notation used for angles, areas, and distances.

Contributions. Due to the Lagrange property of mean value coordinates, the interpolation of data that is given at the vertices of a set of polygons can be done directly and efficiently, without solving a linear system. In the context of transfinite interpolation, the locality of the coordinate functions further enables a simple and progressive update of the solution if the sampling density is increased. Interestingly, the interpolating surfaces are often strikingly similar to interpolating thin plate splines, even though they require far less computational effort.

3. GENERAL CONSTRUCTION OF HOMOGENEOUS BARYCENTRIC COORDINATES

Let Ψ be an arbitrary simple polygon in the plane with $n \geq 3$ distinct vertices v_1, \dots, v_n and nonintersecting (open) edges $e_i = (v_i, v_{i+1}) = \{(1 - \mu)v_i + \mu v_{i+1} : 0 < \mu < 1\}$ (see Figure 1(a)–(c) for some examples). The situation in Figure 1(d), where Ψ is a set of (possibly nested) simple polygons, will be discussed in Section 4. For $i = 1, \dots, n$ we define for any $v \in \mathbb{R}^2$ the usual Euclidean distance to v_i as $r_i(v) = \|v_i - v\|$ and denote by $\alpha_i(v)$ the *signed* angle in the triangle $[v, v_i, v_{i+1}]$ at vertex v . Then,

$$A_i(v) = r_i(v)r_{i+1}(v)\sin(\alpha_i(v))/2 \quad (5)$$

and

$$B_i(v) = r_{i-1}(v)r_{i+1}(v)\sin(\alpha_{i-1}(v) + \alpha_i(v))/2 \quad (6)$$

are the signed areas of the triangles $[v, v_i, v_{i+1}]$ and $[v, v_{i-1}, v_{i+1}]$, respectively¹ (see Figure 2). It is now well-known that

$$A_i(v), \quad -B_i(v), \quad A_{i-1}(v)$$

are homogeneous barycentric coordinates of v with respect to the triangle $\Delta_i = [v_{i-1}, v_i, v_{i+1}]$. In other words,

$$A_i(v)(v_{i-1} - v) - B_i(v)(v_i - v) + A_{i-1}(v)(v_{i+1} - v) = 0. \quad (7)$$

Often, these coordinates are divided by their sum $C_i = A_{i-1}(v) + A_i(v) - B_i(v)$, the area of Δ_i , to give the normalized barycentric coordinates as ratios of areas.

¹Note that we always treat indices cyclically with respect to n , so that $e_n = (v_n, v_1)$ and $B_1(v) = \text{Area}[v, v_n, v_2]$, for example.

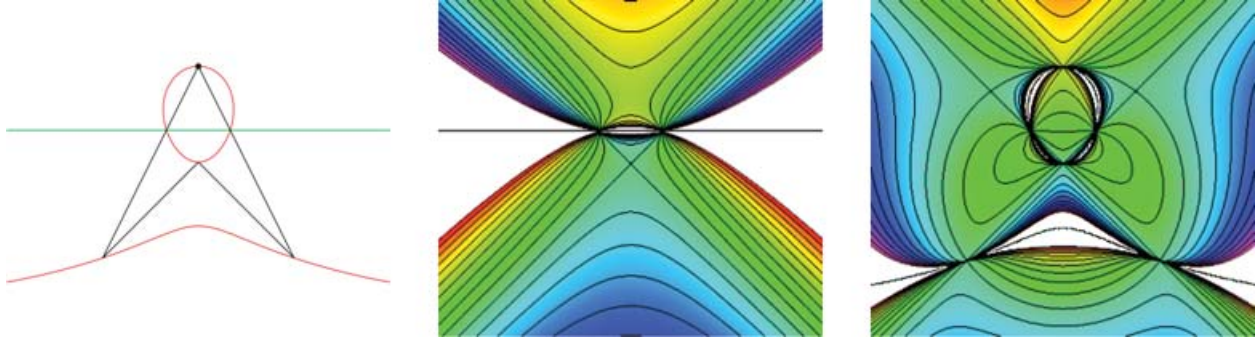


Fig. 3. Zero set of the denominator $W(v)$ for the Wachspress (green) and discrete harmonic coordinates (red) for a concave polygon (left) and contour plots of the normalized Wachspress (middle) and discrete harmonic (right) coordinate function λ_i that corresponds to the topmost vertex.

Let us now consider the homogeneous coordinates of v with respect to all triangles $\Delta_1, \dots, \Delta_n$. Then, we have for any vertex v_i of Ψ three coordinates that correspond to v_i , one in each of the three triangles Δ_{i-1} , Δ_i , and Δ_{i+1} . If we now take a weighted average of these three coordinates and define

$$w_i(v) = b_{i-1}(v)A_{i-2}(v) - b_i(v)B_i(v) + b_{i+1}(v)A_{i+1}(v), \quad (8)$$

where the weight functions $b_i : \mathbb{R}^2 \rightarrow \mathbb{R}$ can be chosen arbitrarily, then it follows from Eq. (7) that the functions w_i are homogeneous barycentric coordinates with respect to Ψ because

$$\sum_{i=1}^n w_i(v)(v_i - v) = \sum_{i=1}^n b_i(v)(A_i(v)(v_{i-1} - v) - B_i(v)(v_i - v) + A_{i+1}(v)(v_{i+1} - v)) = 0.$$

The critical part now is the normalization of these homogeneous coordinates, that is, to guarantee that the denominator in Eq. (3) is nonzero for every $v \in \mathbb{R}^2$. For convex polygons this is relatively easy to achieve. Indeed, it follows from Eq. (8) that

$$W(v) = \sum_{i=1}^n w_i(v) = \sum_{i=1}^n b_i(v)C_i, \quad (9)$$

and since all C_i have the same sign if Ψ is convex, $W(v)$ can never be zero, as long as all the weight functions b_i are positive (or negative). But in the general case, it is more difficult to avoid dividing by zero. Consider, for example, Wachspress and discrete harmonic coordinates that can be generated by the weight functions

$$b_i^W = \frac{1}{A_{i-1}A_i} \quad \text{and} \quad b_i^D = \frac{r_i^2}{A_{i-1}A_i}.$$

Both coordinates are well-defined for v inside any convex polygon. However, inside a nonconvex polygon, $W(v)$ can be zero, and the normalized coordinates $\lambda_i(v)$ may have nonremovable poles, as illustrated for a concave quadrilateral in Figure 3.

To avoid this problem, Eq. (9) suggests taking weight functions like $b_i = 1/C_i$ so that $W \equiv n$. But although this particular choice gives well-defined (and linear) normalized coordinates λ_i as long as no three consecutive vertices of Ψ are collinear, they unfortunately do not satisfy Eq. (4). Another option that gives the metric coordinates [Sukumar and Malsch 2006] is

$$b_i^M = \frac{1}{C_i q_{i-1} q_i},$$

where the positivity of the functions $q_i = r_i + r_{i+1} - \|v_{i+1} - v_i\|$ guarantees a nonvanishing denominator $W(v)$. The corresponding normalized coordinates satisfy the Lagrange property, but like discrete harmonic coordinates, they are not necessarily bounded between 0 and 1 inside a convex polygon. Thus, an interpolating function may take on values outside the convex hull of the given data, which can be undesirable in some applications.

In this article we want to study the mean value coordinates which are generated by the weight functions

$$b_i^{MV} = \frac{r_i}{A_{i-1}A_i}.$$

With this particular choice of b_i , Eq. (8) becomes

$$w_i = \frac{r_{i-1}A_i - r_iB_i + r_{i+1}A_{i-1}}{A_{i-1}A_i}, \quad (10)$$

which is the formula given by Floater et al. [2006]. By using Eqs. (5) and (6), in addition to some trigonometric identities, this simplifies to

$$w_i = 2 \frac{\tan(\alpha_{i-1}/2) + \tan(\alpha_i/2)}{r_i}, \quad (11)$$

which (up to the factor 2) is the formula that originally appeared in Floater [2003]. Note that these w_i are three-point coordinates [Floater et al. 2006] in the sense that w_i depends only on v_i and its two neighbors v_{i-1} and v_{i+1} . The same holds for Wachspress and discrete harmonic coordinates, but not for metric coordinates, which depend on v_{i-2}, \dots, v_{i+2} and therefore are *five-point coordinates*.

4. PROPERTIES OF MEAN VALUE COORDINATES

To study the behavior of the mean value coordinates w_i from Eq. (11), let us first assume that $v \in \mathbb{R}^2 \setminus \Psi$, where Ψ is a simple polygon or a set of (possibly nested) simple polygons. Then it follows that $-\pi < \alpha_i(v) < \pi$ and $r_i(v) > 0$ for $i = 1, \dots, n$, so that all homogeneous coordinate functions w_i from Eq. (11) are well-defined. Under these conditions, we can show the following refinement rule.

LEMMA 4.1. *Let $\hat{v} = (1 - \mu)v_j + \mu v_{j+1}$ with $0 < \mu < 1$ be some point on the edge e_j . If we refine the polygon Ψ to $\hat{\Psi}$ by adding \hat{v} between v_j and v_{j+1} (see Figure 4) and denote the homogeneous coordinates with respect to $\hat{\Psi}$ by $\hat{w}_1, \dots, \hat{w}_n$ and \hat{w} , then we have $w_j = \hat{w}_j + (1 - \mu)\hat{w}$, $w_{j+1} = \hat{w}_{j+1} + \mu\hat{w}$, and $w_i = \hat{w}_i$ for $i \neq j, j + 1$.*

PROOF. For $i \neq j, j + 1$, the statement follows directly from the fact that the mean value coordinates are three-point coordinates. According to Eq. (11), the remaining three homogeneous coordinates of $\hat{\Psi}$ are

$$\begin{aligned} \hat{w}_j &= 2(\tan(\alpha_{j-1}/2) + \tan(\hat{\alpha}^-/2))/r_j, \\ \hat{w} &= 2(\tan(\hat{\alpha}^-/2) + \tan(\hat{\alpha}^+/2))/\hat{r}, \\ \hat{w}_{j+1} &= 2(\tan(\hat{\alpha}^+/2) + \tan(\alpha_{j+1}/2))/r_{j+1}. \end{aligned}$$

If v , v_j , and v_{j+1} are collinear, then $\alpha_j = \hat{\alpha}^- = \hat{\alpha}^+ = 0$ and it is easy to verify that $\hat{w}_j = w_j$, $\hat{w} = 0$, and $\hat{w}_{j+1} = w_{j+1}$. Otherwise, all three angles are nonzero and we can write $(1 - \mu)$ and μ as ratios of areas

$$1 - \mu = \frac{\text{Area}[v, \hat{v}, v_{j+1}]}{\text{Area}[v, v_j, v_{j+1}]} = \frac{\hat{r} \sin \hat{\alpha}^+}{r_j \sin \alpha_j} \quad \text{and} \quad \mu = \frac{\text{Area}[v, v_j, \hat{v}]}{\text{Area}[v, v_j, v_{j+1}]} = \frac{\hat{r} \sin \hat{\alpha}^-}{r_{j+1} \sin \alpha_j}.$$

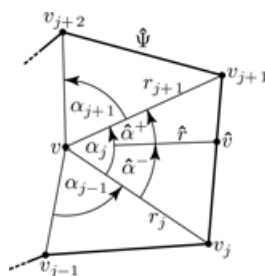


Fig. 4. Notation used in Lemma 4.1 for the refinement of Ψ to $\hat{\Psi}$.

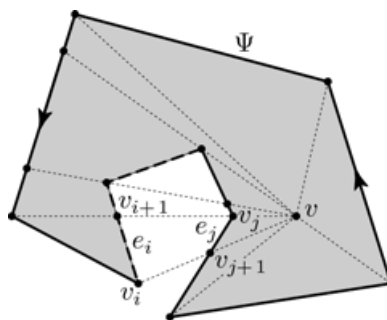


Fig. 5. Partitioning into sectors with exit (solid) and entry edges (dashed).

We then find that

$$\frac{r_j}{2}(w_j - \hat{w}_j - (1 - \mu)\hat{w}) = \tan(\alpha_j/2) - \tan(\hat{\alpha}^-/2) - \frac{\sin \hat{\alpha}^+}{\sin \alpha_j}(\tan(\hat{\alpha}^-/2) + \tan(\hat{\alpha}^+/2)),$$

and

$$\frac{r_{j+1}}{2}(w_{j+1} - \hat{w}_{j+1} - \mu \hat{w}) = \tan(\alpha_j/2) - \tan(\hat{\alpha}^+/2) - \frac{\sin \hat{\alpha}^-}{\sin \alpha_j}(\tan(\hat{\alpha}^-/2) + \tan(\hat{\alpha}^+/2)),$$

where both righthand-sides simplify to zero after using first the identity $\tan(x/2) = (1 - \cos x)/\sin x$ and then the sine and cosine addition formulae for $\alpha_j = \hat{\alpha}^- + \hat{\alpha}^+$. \square

An immediate consequence of this refinement rule is that the sum of homogeneous coordinates does not change under this kind of refinement.

COROLLARY 4.2. *If Ψ is refined to $\hat{\Psi}$ as in Lemma 4.1, then $W = \hat{W}$.*

But it is even more important that this sum never vanishes.

THEOREM 4.3. *The sum $W(v)$ of the homogeneous mean value coordinates of Eq. (11) is nonzero for all $v \notin \Psi$.*

PROOF. Let us first assume that Ψ is a single simple polygon with positive orientation and that v lies in the interior of Ψ . We then consider the rays from v through the vertices v_i and add all intersection points of the rays with the edges of the polygon to Ψ , as shown in Figure 5. According to Corollary 4.2, this does not change $W(v)$. Next, we consider for any of the radial sectors between two neighboring rays all edges inside the sector and classify them as *exit edges* (solid) or *entry edges* (dashed), depending on

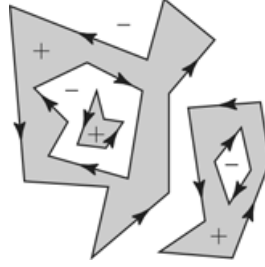


Fig. 6. Orientation (arrows), interior (gray), and sign of W (+/-) for a set of simple polygons.

whether a traveler coming from v exits or enters the interior of Ψ at the edge. If we define for each edge $e_i = (v_i, v_{i+1})$, the value

$$\kappa_i = \left(\frac{1}{r_i} + \frac{1}{r_{i+1}} \right) \tan(\alpha_i/2),$$

then it follows from the orientation of Ψ that κ_i is positive if e_i is an exit edge and negative if e_i is an entry edge. And for edges e_i that lie on one of the rays, we have $\kappa_i = 0$.

Now let e_i be one of the entry edges. Then there always exists an exit edge e_j in the same sector that is closer to v (see Figure 5). But as $\alpha_i = -\alpha_j$ and at least one of the inequalities $r_j \leq r_{i+1}$ and $r_{j+1} \leq r_i$ is strict, we have

$$\kappa_j = \left(\frac{1}{r_j} + \frac{1}{r_{j+1}} \right) \tan(\alpha_j/2) > \left(\frac{1}{r_i} + \frac{1}{r_{i+1}} \right) \tan(-\alpha_i/2) = -\kappa_i.$$

This means that the negative κ_i of entry edge e_i is counterbalanced by the positive κ_j of exit edge e_j . As this holds for all entry edges (without using any exit edge twice), we conclude that

$$\sum_{i=1}^n \kappa_i > 0.$$

However, the sum of the κ_i can be rearranged, by a change of summation index, to be half the sum of the w_i from Eq. (11) and therefore $W(v)$ is positive for any v inside Ψ . Likewise, we can show that W is negative over the exterior of Ψ , and vice versa if Ψ is negatively oriented.

If Ψ is a set of (possibly nested) simple polygons, then the same lines of argument hold, as long as the entry and exit edges keep alternating in each radial sector. But this can easily be guaranteed by requiring the orientation of single polygons to alternate, as shown in Figure 6. If we further define the interior of such a set of polygons to be the regions “left” of the polygons (marked gray in Figure 6), then it follows that W is positive over the interior of Ψ , and negative otherwise. \square

A consequence of Theorem 4.3 is that the normalization in Eq. (3) is well-defined for arbitrary planar polygons without self-intersections. And as the normalized mean value coordinates λ_i are a composition of analytic functions, it follows that they are C^∞ over the open set $\mathbb{R}^2 \setminus \Psi$. However, the question remains whether the λ_i have a continuous extension to the whole plane and satisfy the Lagrange property of Eq. (4). In the case of convex polygons, the answer to both questions is positive and moreover, the λ_i are linear along the edges of Ψ [Floater et al. 2006]. We will now show that this also holds for arbitrary polygons.

THEOREM 4.4. *Let $v^* = (1 - \mu)v_j + \mu v_{j+1}$ with $0 < \mu < 1$ be some point on the edge e_j of Ψ . Then the normalized mean value coordinates λ_i converge to $(1 - \mu)\delta_{i,j} + \mu\delta_{i,j+1}$ at v^* .*

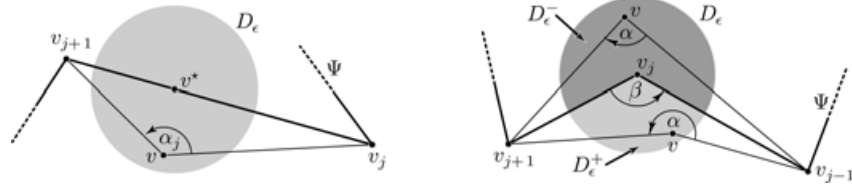


Fig. 7. Notation used in the proofs of Theorem 4.4 (left) and Theorem 4.6 (right).

PROOF. Let us consider the open disk $D_\epsilon = D_\epsilon(v^*) = \{x \in \mathbb{R}^2 : \|x - v^*\| < \epsilon\}$ around v^* with $\epsilon > 0$ such that D_ϵ does not contain v_j and v_{j+1} and does not intersect any edges of Ψ other than e_j (see Figure 7). Then $w_i(v)$ with $i \neq j, j+1$ is well-defined for any $v \in D_\epsilon$ and only w_j and w_{j+1} have poles for $v \in D_\epsilon \cap e_j$. To remove these poles, we consider the slightly modified functions $\tilde{w}_i = w_i A_j / 2$. For $i \neq j, j+1$, these are still well-defined functions over D_ϵ with $\tilde{w}_i(v) = 0$ for $v \in D_\epsilon \cap e_j$. Furthermore, we have

$$\tilde{w}_j = 2 \frac{\tan(\alpha_{j-1}/2) + \tan(\alpha_j/2)}{r_j} \frac{r_j r_{j+1} \sin \alpha_j}{4} = \frac{r_{j+1}}{2} (\tan(\alpha_{j-1}/2) \sin \alpha_j + (1 - \cos \alpha_j))$$

and likewise

$$\tilde{w}_{j+1} = \frac{r_j}{2} (\tan(\alpha_{j+1}/2) \sin \alpha_j + (1 - \cos \alpha_j)),$$

which are both well-defined everywhere in D_ϵ . In particular, for any $v \in D_\epsilon \cap e_j$, we have $\sin \alpha_j(v) = 0$ and $\cos \alpha_j(v) = -1$ so that $\tilde{w}_j(v) = r_{j+1}(v)$ and $\tilde{w}_{j+1}(v) = r_j(v)$.

When we normalize the functions \tilde{w}_i as in Eq. (3), then the common factor $A_j/2$ cancels out and we get functions $\tilde{\lambda}_i$ that agree with λ_i for any $v \in D_\epsilon \setminus e_j$, that is,

$$\tilde{\lambda}_i(v) = \frac{\tilde{w}_i(v)}{\sum_{k=1}^n \tilde{w}_k(v)} = \frac{w_i(v) A_j(v) / 2}{\sum_{k=1}^n w_k(v) A_j(v) / 2} = \frac{w_i(v)}{\sum_{k=1}^n w_k(v)} = \lambda_i(v).$$

The advantage of the $\tilde{\lambda}_i$ is that they are also well-defined over $D_\epsilon \cap e_j$, so that we have

$$\lim_{v \rightarrow v^*} \lambda_i(v) = \tilde{\lambda}_i(v^*) = \frac{\tilde{w}_i(v^*)}{\sum_{k=1}^n \tilde{w}_k(v^*)} = \frac{\delta_{i,j} r_{j+1}(v^*) + \delta_{i,j+1} r_j(v^*)}{r_{j+1}(v^*) + r_j(v^*)}$$

and the proof is completed by noting that $r_j(v^*) = \mu \|v_j - v_{j+1}\|$ and $r_{j+1}(v^*) = (1 - \mu) \|v_j - v_{j+1}\|$. \square

Remark 4.5. Note that functions $\tilde{\lambda}_i$ are composed of analytic functions and thus are C^∞ over $D_\epsilon(v^*)$.

THEOREM 4.6. *The normalized mean value coordinates λ_i converge to $\delta_{i,j}$ at v_j .*

PROOF. Let us consider again a small open disk D_ϵ around v_j that intersects only the edges e_{j-1} and e_j of Ψ , so that $D_\epsilon \setminus \Psi$ decomposes into the two open sets D_ϵ^+ and D_ϵ^- (see Figure 7). We further choose ϵ small enough such that D_ϵ does not intersect the infinite straight line through v_{j-1} and v_{j+1} , which in turn guarantees that $w_j(v) \neq 0$ for all $v \in D_\epsilon \setminus \Psi$. Dividing both the numerator and denominator of λ_i by w_j then gives

$$\lambda_i = \frac{(w_i/w_j)}{1 + \sum_{k \neq j} (w_k/w_j)} \quad \text{for } i \neq j \quad \text{and} \quad \lambda_j = \frac{1}{1 + \sum_{k \neq j} (w_k/w_j)},$$

and so it is sufficient to show that $w_i(v)/w_j(v)$ converges to 0 at v_j for all $i \neq j$. Using the identity $\tan x + \tan y = \sin(x + y)/(\cos x \cos y)$, we have $w_i/w_j = (r_j/r_i)R_{ij}$ with

$$R_{ij} = \frac{\sin((\alpha_{i-1} + \alpha_i)/2) \cos(\alpha_{j-1}/2) \cos(\alpha_j/2)}{\sin((\alpha_{j-1} + \alpha_j)/2) \cos(\alpha_{i-1}/2) \cos(\alpha_i/2)}, \quad (12)$$

and since $\lim_{v \rightarrow v_j} r_j(v) = 0$ and $\lim_{v \rightarrow v_j} r_i(v) = \|v_i - v_j\| > 0$ for $i \neq j$, it is sufficient to show that R_{ij} is bounded in absolute value over $D_\epsilon \setminus \Psi$ for $i \neq j$. As the numerator in this quotient is clearly bounded in absolute value by 1, even though not all terms necessarily converge at v_j , it remains to show that the denominator is bounded away from zero.

For $i \neq j - 1, j$, the angle functions α_i are clearly continuous over D_ϵ with $-\pi < \alpha_i(v) < \pi$, and thus $\cos(\alpha_i(v)/2) > 0$ for all $v \in D_\epsilon$. The remaining two angle functions α_{j-1} and α_j , on the other hand, are continuous over $D_\epsilon \setminus \Psi$, but not well-defined at v_j . However, by considering the quadrilateral $(v_{j-1}, v_j, v_{j+1}, v)$ and noting that the angles of this quadrilateral at v_{j-1} and v_{j+1} vanish as v converges to v_j , it is easy to see that the sum $\alpha(v) = \alpha_{j-1}(v) + \alpha_j(v)$ converges to $2\pi - \beta$ for $v \in D_\epsilon^+$ and to $-\beta$ for $v \in D_\epsilon^-$ with β as in Figure 7. Therefore, the function $|\sin((\alpha_{j-1} + \alpha_j)/2)|$ is continuous over $D_\epsilon^+ \cup D_\epsilon^- \cup \{v_j\}$ with

$$\lim_{v \rightarrow v_j} |\sin((\alpha_{j-1}(v) + \alpha_j(v))/2)| = |\sin(\beta/2)| > 0,$$

so that the term $\sin((\alpha_{j-1} + \alpha_j)/2)$ is guaranteed to be bounded away from zero over $D_\epsilon \setminus \Psi$. The two observations together immediately show that the denominator of R_{ij} in Eq. (12) is bounded away from zero for $i \neq j - 1, j + 1$. However, the same arguments also hold if $i = j - 1$ because R_{ij} then simplifies by cancellation to

$$R_{j-1,j} = \frac{\sin((\alpha_{j-2} + \alpha_{j-1})/2) \cos(\alpha_j/2)}{\sin((\alpha_{j-1} + \alpha_j)/2) \cos(\alpha_{j-2}/2)}$$

and similarly in the remaining case $i = j + 1$. \square

With these results, we can now give a precise definition of the normalized mean value coordinates for arbitrary planar polygons and summarize their properties.

Definition 4.7. For any set of simple polygons Ψ , we call the functions $\lambda_i : \mathbb{R}^2 \rightarrow \mathbb{R}$ for $i = 1, \dots, n$ with

$$\lambda_i(v) = \begin{cases} \frac{w_i(v)}{\sum_{j=1}^n w_j(v)} & \text{if } v \notin \Psi \text{ with } w_i, \text{ as defined in Eq. (11),} \\ (1 - \mu)\delta_{i,j} + \mu\delta_{i,j+1} & \text{if } v = (1 - \mu)v_j + \mu v_{j+1} \in e_j, \\ \delta_{i,j} & \text{if } v = v_j \end{cases} \quad (13)$$

the mean value coordinates of Ψ .

COROLLARY 4.8. The mean value coordinates λ_i have the following properties:

- (1) **Affine precision:** $\sum_{i=1}^n \lambda_i \varphi(v_i) = \varphi$ for any affine function $\varphi : \mathbb{R}^2 \rightarrow \mathbb{R}^d$.
- (2) **Lagrange property:** $\lambda_i(v_j) = \delta_{i,j}$.
- (3) **Smoothness:** λ_i is C^∞ everywhere, except at the vertices v_j , where it is only C^0 .
- (4) **Partition of unity:** $\sum_{i=1}^n \lambda_i \equiv 1$.
- (5) **Similarity invariance:** if $\varphi : \mathbb{R}^2 \rightarrow \mathbb{R}^2$ is a similarity² and $\hat{\Psi} = \varphi(\Psi)$, then $\lambda_i(v) = \hat{\lambda}_i(\varphi(v))$.

²A transformation is called a similarity if it is a translation, rotation, reflection, uniform scaling, or combination of these.



Fig. 8. In this example, Ψ is a set of four simple polygons. The contour plots visualize the three mean value coordinates λ_i that correspond to the vertices marked by fat dots.

- (6) **Linear independence:** if $\sum_{i=1}^n c_i \lambda_i(v) = 0$ for all $v \in \mathbb{R}^2$, then all c_i must be zero.
- (7) **Refinability:** if we refine Ψ to $\hat{\Psi}$ by splitting e_j at $\hat{v} = (1 - \mu)v_j + \mu v_{j+1}$, then $\lambda_j = \hat{\lambda}_j + (1 - \mu)\hat{\lambda}$, $\lambda_{j+1} = \hat{\lambda}_{j+1} + \mu\hat{\lambda}$, and $\lambda_i = \hat{\lambda}_i$ for $i \neq j, j + 1$.
- (8) **Edge property:** λ_i is linear along the edges e_j of Ψ .
- (9) **Positivity:** λ_i is positive inside the kernel of star-shaped polygons, in particular, inside convex polygons.

PROOF. (1) follows from Eqs. (8) and (3) and implies (4) with $\phi \equiv 1$. Furthermore, (2), (8), and (9) follow directly from the definitions in Eqs. (13) and (11) and (3) from Theorems 4.4 and 4.6 and Remark 4.5. We conclude (5) from the fact that the w_i in Eq. (11) depend only on angles and distances and that any uniform scale factor cancels out by the normalization. Finally, (6) can be deduced from (2) and (7) follows from Lemma 4.1. \square

Figure 8 illustrates the typical behavior of the mean value coordinates for a set of simple polygons.

Note that most of these properties (in particular the affine precision and the Lagrange property) can also be derived from the integral construction that was used in [Ju et al. 2005] to derive mean value coordinates in three dimensions. But proving that the coordinates are well-defined for concave shapes and smooth across the boundary is less obvious and has not been done so far, to the best of our knowledge.

The main application of these generalized barycentric coordinates is the interpolation of values that are given at the vertices v_i of Ψ . In other words, if a data value $f_i \in \mathbb{R}^d$ is specified at each v_i , then we are interested in the function $F : \mathbb{R}^2 \rightarrow \mathbb{R}^d$ that is defined by

$$F(v) = \sum_{i=1}^n \lambda_i(v) f_i. \quad (14)$$

Due to the Lagrange and edge properties of the coordinates, this function interpolates f_i at v_i and is linear along the edges e_i of Ψ .

An example where the f_i are RGB color values is shown in Figure 9. As the mean value coordinates are not necessarily positive for arbitrary polygons, it can happen that the interpolated RGB values are outside the valid range $[0, 255]$. In this case, we simply truncate the values to 0 or 255, respectively. As a result, the interpolation function F is only C^0 along certain curves and these artifacts are noticeable in the plot. The same holds for interpolation with the metric coordinates of Sukumar and Malsch [2006].

5. IMPLEMENTATION

For the actual computation of the interpolation function F , we basically use the definition in Eq. (13), but we suggest a slight modification for determining the homogeneous coordinates w_i from Eq. (11) that avoids the computation of angles α_i and enables an efficient handling of the special cases that can occur. If we let $s_i(v) = v_i - v$ and denote the dot product of s_i and s_{i+1} by D_i , then we have

$$\tan(\alpha_i/2) = \frac{1 - \cos(\alpha_i)}{\sin(\alpha_i)} = \frac{r_i r_{i+1} - D_i}{2A_i},$$



Fig. 9. Color interpolation with mean value coordinates (left) and metric coordinates (right) for the polygons from Figure 8 and regions where the interpolation of the individual color channels has been truncated for values below 0 (dark shade) and above 255 (light shade).

and we use this formula as long as $A_i(v) \neq 0$. Otherwise, v lies on the line through v_i and v_{i+1} and we distinguish three cases. If $v = v_i$ or $v = v_{i+1}$, then we do not bother to compute the $w_i(v)$ and simply set $F(v) = f_i$ or $F(v) = f_{i+1}$. Likewise, if v lies on the edge e_i , then we use the linearity of F along e_i to determine $F(v)$ directly. Note that we can easily identify this case because it implies $D_i(v) < 0$. Finally, if v is not on Ψ , then we conclude that $\alpha_i(v) = 0$ and therefore $\tan(\alpha_i(v)/2) = 0$.

The pseudocode for computing $F(v)$ is given in Figure 10. To clarify the situation with multiple polygons, we assume that Ψ is a set of m simple polygons Ψ_1, \dots, Ψ_m , where each Ψ_j has n_j vertices $v_{j,1}, \dots, v_{j,n_j}$. Note that indices $(j, i+1) = (j, i^+)$ and $(j, i-1) = (j, i^-)$ are treated cyclically with respect to Ψ_j .

6. APPLICATIONS AND RESULTS

We now present three applications of the mean value coordinates that demonstrate their potential impact on computer graphics and geometric modeling.

6.1 Phong Shading for Arbitrary Polygons

The standard approach to treating an arbitrary polygon in the rendering pipeline is to first tessellate it into triangles and then process each triangle in turn. For example, *OpenGL* automatically splits a pentagonal face into three triangles (possibly depending on the choice of the first vertex). This gives the expected result if flat shading is used, but the splits become visible as soon as Gouraud or Phong shading is turned on (see Figure 11(a)–(c)).

Phong shading uses triangular barycentric coordinates to linearly interpolate the normals that are given at the vertices of the face over each generated triangle. This can be seen for the two triangles that are marked by red and blue spots in the Phong-shaded result. Since the lower two vertices of both triangles have identical normals, the interpolated normal, as well as the resulting color value, vary linearly inside the triangles. Instead, we can improve the idea of Phong shading and use mean value coordinates to smoothly interpolate the normals over the whole polygon, giving a much more pleasant rendering result (see Figure 11(d)).

Note that the polygons in this example are flat and extending the mean value interpolation to general 3D polygons would require the use of a 2D reference polygon. This may become difficult to handle for complex polygons, but for the special case of 3D quadrilaterals, Hormann and Tarini [2004] have shown how to effectively use mean value coordinates for rendering and rasterization.

```

function  $F(v)$ 
  for  $j = 1$  to  $m$  do
    for  $i = 1$  to  $n_j$  do
       $s_{j,i} := v_{j,i} - v$ 
    for  $j = 1$  to  $m$  do
      for  $i = 1$  to  $n_j$  do
         $i^+ := (i \bmod n_j) + 1$ 
         $r_{j,i} := \|s_{j,i}\|$ 
         $A_{j,i} := \det(s_{j,i}, s_{j,i^+})/2$ 
         $D_{j,i} := \langle s_{j,i}, s_{j,i^+} \rangle$ 
        if  $r_{j,i} = 0$  then //  $v = v_{j,i}$ 
          return  $f_{j,i}$ 
        if  $A_{j,i} = 0$  and  $D_{j,i} < 0$  then //  $v \in e_{j,i}$ 
           $r_{j,i^+} := \|s_{j,i^+}\|$ 
          return  $(r_{i^+} f_{i^+} + r_i f_i)/(r_i + r_{i^+})$ 
   $f := 0$ 
   $W := 0$ 
  for  $j = 1$  to  $m$  do
    for  $i = 1$  to  $n_j$  do
       $i^+ := (i \bmod n_j) + 1$ 
       $i^- := ((i - 2) \bmod n_j) + 1$ 
       $w := 0$ 
      if  $A_{j,i^-} \neq 0$  then
         $w := w + (r_{j,i^-} - D_{j,i^-}/r_{j,i^-})/A_{j,i^-}$ 
      if  $A_{j,i} \neq 0$  then
         $w := w + (r_{j,i} - D_{j,i}/r_{j,i})/A_{j,i}$ 
       $f := f + w f_{j,i}$ 
       $W := W + w$ 
  return  $f/W$ 

```

Fig. 10. Pseudocode for evaluating the interpolation function.

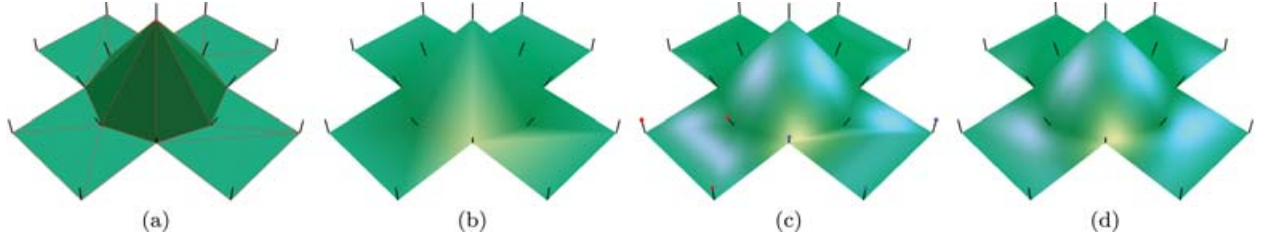


Fig. 11. Rendering of three pentagons with (a) flat, (b) Gouraud, (c) Phong, and (d) generalized Phong shading.

6.2 Image Warping

Another potential application of generalized barycentric coordinates is for image warping, as they offer a particularly simple solution to this problem that can briefly be stated as follows.

Given a rectangular region Ω , a set of *source* polygons Ψ with vertices $v_i \in \Omega$, and a topologically equivalent³ set of *target* polygons $\hat{\Psi}$ with vertices $\hat{v}_i \in \Omega$, we would like to construct a smooth warp function $f : \Omega \rightarrow \Omega$ that maps each v_i to \hat{v}_i . This warp function can then be used to deform a source image $I : \Omega \rightarrow C$ that maps Ω to some color space C into a target image $\hat{I} : \Omega \rightarrow C$ by simply setting $\hat{I} = I \circ f^{-1}$. For practical reasons, the *inverse mapping* $g = f^{-1}$ is often constructed, instead of f .

³ Ψ and $\hat{\Psi}$ must have the same number of components and vertices per component.

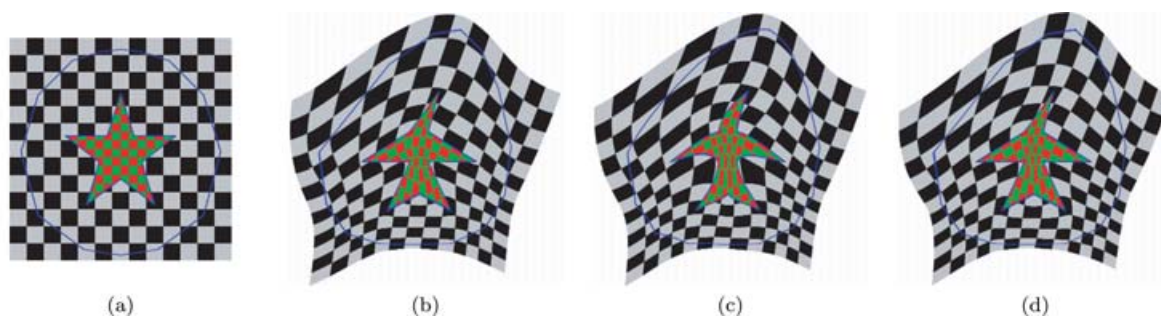


Fig. 12. Warping an image (a) with mean value coordinates (b) and radial basis functions (c) and (d) by moving the vertices of two nested polygons (blue).

Such an inverse warp function can easily be defined with the mean value coordinates $\hat{\lambda}_i$ of $\hat{\Psi}$. It follows immediately from the Lagrange property that the function

$$g(x) = \sum_{i=1}^n \hat{\lambda}_i(x) v_i \quad (15)$$

maps each \hat{v}_i to v_i and thus defines a proper inverse warp function. The warped image can now be generated by simply setting the color of each target pixel x in \hat{I} to the color of the source point $g(x)$ in I . In our examples, we used a simple bilinear interpolation to determine $I(g(x))$ from the 2×2 grid of pixels surrounding $g(x)$.

Like warping with B-splines and radial basis functions with linear precision, this *barycentric warp* reproduces affine transformations. In other words, if $\varphi : \mathbb{R}^2 \rightarrow \mathbb{R}^2$ is an affine transformation and $\hat{\Psi} = \varphi(\Psi)$, then $\hat{I} = I \circ \varphi^{-1}$. Indeed, since $v_i = \varphi^{-1}(\hat{v}_i)$, it follows from the affine precision of the mean value coordinates that $g(x) = \varphi^{-1}(x)$ in Eq. (15).

Another property of the barycentric warp is that it is linear along the edges of the polygons. Figure 12(b) shows the result of warping the image in (a) after moving the vertices of two nested polygons. The exterior polygon with 14 vertices controls the global shape of the warp, while the interior polygon with 10 vertices is used to deform the star. The result is smooth and the star is clearly mapped to a star with straight edges.

For comparison, we also generated the thin plate spline warp (c) using radial basis interpolation with basis function $\phi(r) = r^2 \log r$ (see Arad et al. [1994] for details). This warp does not reproduce the straight edges of the star, but a common trick to overcome this drawback is to sample the edges with additional vertices. For example, by taking 20 samples per edge, we obtained the result in (d). This is very similar to the barycentric warp, but takes considerably longer to compute; 20 seconds for a 600×600 image on a 2.8 Ghz Pentium, while the barycentric warp took less than one second. This is due to the large linear system that needs to be solved and the large number of basis functions that have to be evaluated. In general, if n is the number of vertices in Ψ and k is the number of samples per edge, then solving the linear system with a standard method is an $O(k^3 \cdot n^3)$ operation and evaluating the m pixels of \hat{I} is of order $O(m \cdot k \cdot n)$. Of course, there exist specialized solvers that can reduce the cost for solving the linear system, but the advantage of the barycentric warp is that it does not require any system to be solved and the whole computation is of order $O(m \cdot n)$ only.

We conclude that the barycentric warp is particularly useful whenever straight edges need to be preserved. For example, making the boundary of the rectangular image one of the source and target polygons guarantees that the warped image will be rectangular too (see Figure 13).

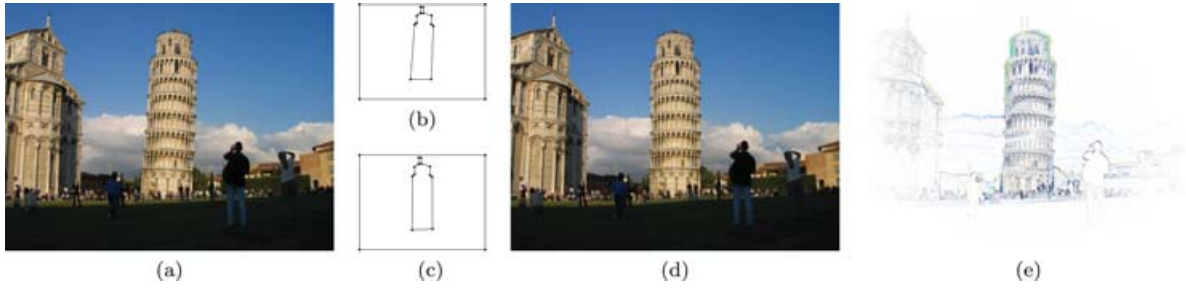


Fig. 13. The Leaning Tower of Pisa (a) can be straightened by a barycentric warp function which maps the two source polygons in (b) to target polygons in (c). The Straight Tower of Pisa is shown in (d) and the difference between the pictures in (e).

6.3 Transfinite Interpolation

The mean value coordinates also provide an efficient solution to the following interpolation problem. Given a set of closed planar curves c_j and some d -dimensional data over these curves $d_j : c_j \rightarrow \mathbb{R}^d$, we would like to have a function $F : \mathbb{R}^2 \rightarrow \mathbb{R}^d$ that interpolates the given data, that is, $F(v) = d_j(v)$ for any $v \in c_j$.

The obvious approach is to approximate the given curves c_j with a set of polygons Ψ whose vertices v_i lie on the curves c_j . Then the function F in Eq. (14) with $f_i = d_j(v_i)$ clearly is an approximate solution of the stated interpolation problem. And as the polygons Ψ converge to the curves c_j by increasing the sampling density, so does function F converge to the desired solution.

The interesting fact now is that the structure of the mean value coordinates allows an efficient update of the solution if the sampling density is increased. Assume that we computed $F(v)$ and also $W(v)$ for some point $v \notin \Psi$, and then refine Ψ to $\hat{\Psi}$ by adding a vertex \hat{v} with data value $\hat{f} = d_j(\hat{v})$ between v_j and v_{j+1} . Then it follows by a consideration very similar to the one in the proof of Lemma 4.1 that

$$w_j = \hat{w}_j + \sigma \hat{w}, \quad w_{j+1} = \hat{w}_{j+1} + \tau \hat{w},$$

and

$$\hat{W} = W + \rho \hat{w}, \quad (16)$$

where $\rho(v)$, $\sigma(v)$, and $\tau(v)$ are the normalized barycentric coordinates⁴ of \hat{v} with respect to the triangle $[v, v_j, v_{j+1}]$ and \hat{w} is the new homogeneous coordinate function corresponding to \hat{v} . We can then write the value of the refined interpolation function \hat{F} at v as

$$\hat{F} = F + \frac{\hat{w}}{\hat{W}}(\hat{f} - \rho F - \sigma f_j - \tau f_{j+1}). \quad (17)$$

Therefore, both $F(v)$ and $W(v)$ can be updated by a computation with constant cost for $v \notin \Psi$. If $v \in \Psi$ and v is either a vertex of Ψ or lies on an edge e_k with $k \neq j$, then we simply have $\hat{F}(v) = F(v)$ by definition. Only if $v \in e_j$ is it required to compute $\hat{F}(v)$ (and possibly $\hat{W}(v)$) from scratch.

In the example in Figure 14, we exploited this recurrence relation as follows. We first sampled the three given curves uniformly with 100 vertices v_i and computed the curve normals n_i at v_i . Then, we evaluated the interpolating function F and sum of homogeneous coordinates W on a regular 512×512 grid, yielding values F_{kl} and W_{kl} with $0 \leq k, l \leq 511$. We finally refined Ψ successively by splitting the edge with the largest approximation error to the curve and updated F_{kl} and W_{kl} according to Eqs. (17)

⁴Note that $\rho(v)$, $\sigma(v)$, and $\tau(v)$ are not well-defined if v , v_j , and v_{j+1} are collinear. In this special case, we conclude that $\hat{w} = 0$, $w_j = \hat{w}_j - 2 \tan(\hat{\alpha}^-/2)/r_j$, and $w_{j+1} = \hat{w}_{j+1} - 2 \tan(\hat{\alpha}^+/2)/r_{j+1}$, leading to slightly different update formulae for \hat{F} and \hat{W} .

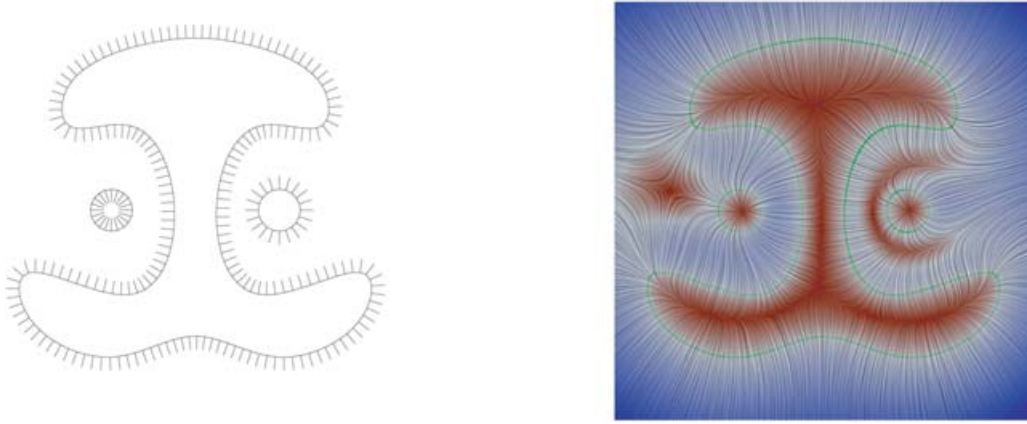


Fig. 14. Three curves with normal vectors (left) and a LIC visualization of the interpolated vector field (right). The color refers to the length ℓ of the vectors (white: $\ell = 1$; blue: $\ell > 1$; red: $\ell < 1$).

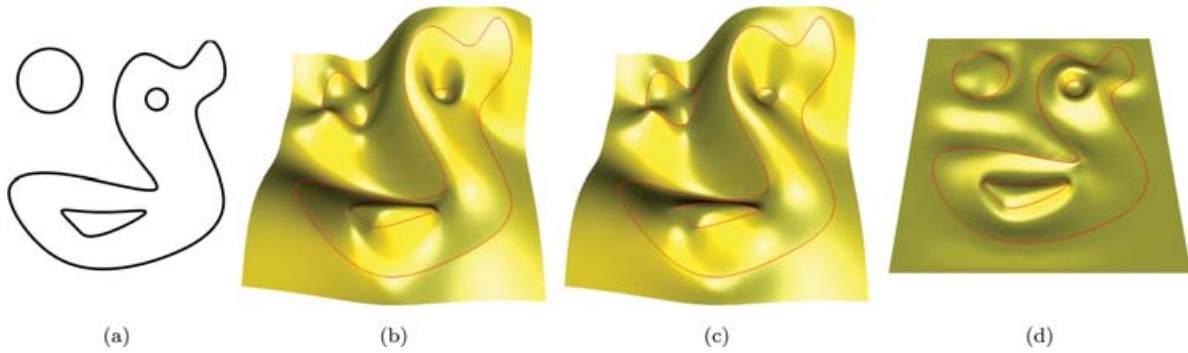


Fig. 15. Interpolation of height values (red) that are given as smooth functions over the four curves in (a) with mean value coordinates (b) and with a thin plate spline (c). The difference of both surfaces is shown in (d).

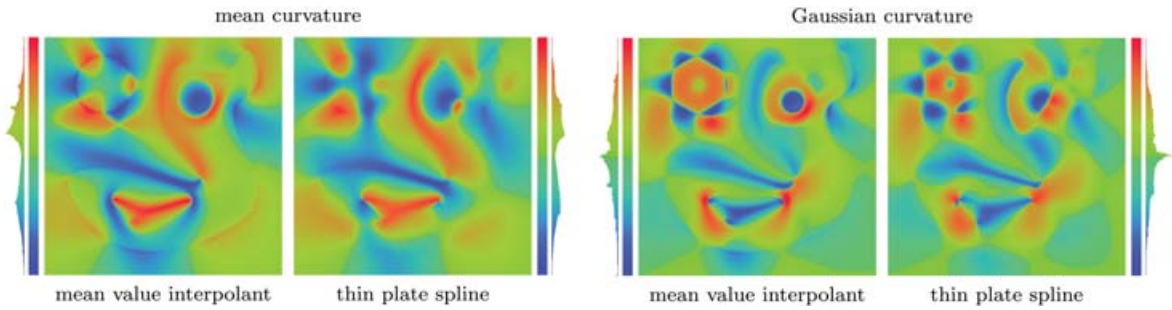


Fig. 16. Discrete curvature plots with histograms for the mean value interpolant and thin plate spline from Figure 15 (b) and (c).

and (16). We stopped the refinement process as soon as $\max_{k,l} \|\hat{F}_{kl} - F_{kl}\| < 0.001$, that is, when the maximum update went below 0.1% of the length of the given vectors. The final polygon consisted of 357 vertices and it took about 10 seconds to compute the final values F_{kl} .

Another example where we interpolated height data is shown in Figure 15. We uniformly sampled the four curves with 2,500 vertices and evaluated the interpolating function over a regular 500×500 grid, which took about 62 seconds. A comparison to the interpolating thin plate spline⁵ showed that the height difference between both surfaces was less than 10% of the maximum value. Using standard finite differencing, we also computed discrete curvature plots for both surfaces (see Figure 16), which reveal a very similar behavior, but it is hard to judge which is preferable.

7. CONCLUSIONS

We have shown that mean value coordinates naturally generalize the concept of triangular barycentric coordinates to arbitrary polygons without intersections, and even to sets of such polygons. Mean value coordinates have a number of important properties and are particularly useful for the interpolation of data that is given at the vertices of the input polygons. As shown in Figures 12, 15, and 16, the behavior of the interpolant is similar to that of thin plate splines, but it can be evaluated directly in $O(n)$ operations without having to solve the fitting problem first. In our implementation, we have typically seen around 10,000,000 evaluations of the coordinates λ_i per second.

We note that in contrast to Sibson's [1980, 1981] coordinates for scattered data, the mean value coordinates have global support and are not everywhere positive in the case of arbitrary polygons. On the other hand, it is probably due to these properties that the interpolants behave so nicely. In the context of image warping, this lack of positivity means that the barycentric warp function is not guaranteed to be one-to-one, except if both the source and target polygons are convex. Nevertheless, the method appears to work very well in practice.

REFERENCES

- ARAD, N., DYN, N., REISFELD, D., AND YESHURUN, Y. 1994. Image warping by radial basis functions: Application to facial expressions. *CVGIP: Graph. Models and Image Proc.* 56, 2, 161–172.
- BEATSON, R. K., LIGHT, W. A., AND BILLINGS, S. 2000. Fast solution of the radial basis function interpolation equations: Domain decomposition methods. *SIAM J. Sci. Comput.* 22, 5, 1717–1740.
- BEATSON, R. K. AND NEWSAM, G. N. 1992. Fast evaluation of radial basis functions: I. *Comput. Math. Appl.* 24, 12, 7–19.
- BUHMANN, M. 2000. Radial basis functions: The state-of-the-art and new results. *Acta Numer.* 9, 1–37.
- CEVA, G. 1678. *De lineis rectis se invicem secantibus, statica constructio*. Ludovici Montiae, Mediolanum.
- CHAI, J., MIYOSHI, T., AND NAKAMAE, E. 1998. Contour interpolation and surface reconstruction of smooth terrain models. In *Proceedings of the Conference on Visualization*. 27–33.
- ECK, M., DEROSE, T., DUCHAMP, T., HOPPE, H., LOUNSBURY, M., AND STUETZLE, W. 1995. Multiresolution analysis of arbitrary meshes. In *Proceedings of the 22nd Annual Conference on Computer Graphics and Interactive Techniques*. 173–182.
- FARIN, G. 1990. Surfaces over Dirichlet tessellations. *Computer Aided Geom. Des.* 7, 1–4, 281–292.
- FARIN, G. 2002. *Curves and Surfaces for CAGD: A Practical Guide*, 5th ed. Morgan Kaufmann Series in Computer Graphics and Geometric Modeling. Morgan Kaufmann, San Francisco.
- FLOATER, M. S. 1997. Parameterization and smooth approximation of surface triangulations. *Comput. Aided Geom. Des.* 14, 3, 231–250.
- FLOATER, M. S. 2003. Mean value coordinates. *Comput. Aided Geom. Des.* 20, 1, 19–27.
- FLOATER, M. S., HORMANN, K., AND KÓS, G. 2006. A general construction of barycentric coordinates over convex polygons. *Adv. Comp. Math.* 24, 1–4, 311–331.
- FLOATER, M. S., KÓS, G., AND REIMERS, M. 2005. Mean value coordinates in 3D. *Comput. Aided Geom. Des.* 22, 7, 623–631.
- GLASBEY, C. A. AND MARDIA, K. V. 1998. A review of image warping methods. *J. Appl. Statistics* 25, 2, 155–171.
- GROSS, L. AND FARIN, G. 1999. A transfinite form of Sibson's interpolant. *Disc. Appl. Math.* 93, 1, 33–50.
- HIYOSHI, H. AND SUGIHARA, K. 2000. Voronoi-Based interpolation with higher continuity. In *Proceedings of the 16th Annual Symposium on Computational Geometry*. 242–250.

⁵We thank Rick Beatson for providing us with the thin plate solution.

- HORMANN, K. AND TARINI, M. 2004. A quadrilateral rendering primitive. In *Graphics Hardware 2004*. T. Akenine-Möller and M. McCool, Eds. Eurographics Association, 7–14.
- JU, T., SCHAEFER, S., AND WARREN, J. 2005. Mean value coordinates for closed triangular meshes. *ACM Trans. Graph.* 24, 3, 561–566.
- JU, T., SCHAEFER, S., WARREN, J., AND DESBRUN, M. 2005. A geometric construction of coordinates for convex polyhedra using polar duals. In *Geometry Processing 2005*. M. Desbrun and H. Pottmann, Eds. Eurographics Association, 181–186.
- KOUNCHEV, O. 2001. *Multivariate Polysplines: Applications to Numerical and Wavelet Analysis*. Academic Press, Orlando, FL.
- LEE, S., CHWA, K.-Y., SHIN, S. Y., AND WOLBERG, G. 1995. Image metamorphosis using snakes and free-form deformations. In *Proceedings of the 22nd Annual Conference on Computer Graphics and Interactive Techniques*. 439–448.
- LEE, S., WOLBERG, G., AND SHIN, S. Y. 1997. Scattered data interpolation with multilevel B-splines. *IEEE Trans. Visual. Comput. Graph.* 3, 3, 228–244.
- MALSCH, E. A. AND DASGUPTA, G. 2004a. Interpolations for temperature distributions: A method for all non-concave polygons. *Int. J. Solids and Structures* 41, 8, 2165–2188.
- MALSCH, E. A. AND DASGUPTA, G. 2004b. Shape functions for polygonal domains with interior nodes. *Int. J. Numer. Method Eng.* 61, 8, 1153–1172.
- MALSCH, E. A. AND DASGUPTA, G. 2005. Algebraic construction of smooth interpolants on polygonal domains. *Mathematica J.* 9, 3, 641–658.
- MALSCH, E. A., LIN, J. J., AND DASGUPTA, G. 2005. Smooth two dimensional interpolants: A recipe for all polygons. *J. Graph. Tools* 10, 2, 27–39.
- MEYER, M., LEE, H., BARR, A. H., AND DESBRUN, M. 2002. Generalized barycentric coordinates on irregular polygons. *J. Graph. Tools* 7, 1, 13–22.
- MILLIRON, T., JENSEN, R. J., BARZEL, R., AND FINKELSTEIN, A. 2002. A framework for geometric warps and deformations. *ACM Trans. Graph.* 21, 1, 20–51.
- MÖBIUS, A. F. 1827. *Der Barycentrische Calcul*. Johann Ambrosius Barth, Leipzig.
- NÜRNBERGER, G. AND ZEILFELDER, F. 2000. Developments in bivariate spline interpolation. *J. Comput. Appl. Math.* 121, 1–2, 125–152.
- PINKALL, U. AND POLTHIER, K. 1993. Computing discrete minimal surfaces and their conjugates. *Experim. Math.* 2, 1, 15–36.
- RUPRECHT, D. AND MÜLLER, H. 1995. Image warping with scattered data interpolation. *Comput. Graph. Appl.* 15, 2, 37–43.
- SIBSON, R. 1980. A vector identity for the Dirichlet tessellation. *Math. Proc. Cambridge Phil. Soc.* 87, 151–155.
- SIBSON, R. 1981. A brief description of natural neighbour interpolation. In *Interpolating Multivariate Data*. V. Barnett, Ed. Wiley, New York, 21–36.
- SUKUMAR, N. AND MALSCH, E. A. 2006. Recent advances in the construction of polygonal finite element interpolants. *Arch. Comput. Meth. Eng.* 13, 1, 129–163.
- WACHSPRESS, E. L. 1975. *A Rational Finite Element Basis*. Academic Press, New York.
- WARREN, J. 1996. Barycentric coordinates for convex polytopes. *Advances in Comput. Math.* 6, 2, 97–108.
- WARREN, J. 2003. On the uniqueness of barycentric coordinates. In *Topics in Algebraic Geometry and Geometric Modeling*. R. Goldman and R. Krasauskas, Eds. Contemporary Mathematics, vol. 334. American Mathematical Society, 93–99.
- WARREN, J., SCHAEFER, S., HIRANI, A. N., AND DESBRUN, M. 2004. Barycentric coordinates for convex sets. Tech. Rep., Rice University.
- WOLBERG, G. 1990. *Digital Image Warping*. IEEE Computer Society Press, Los Alamitos, CA.

Received October 2005; revised March 2006; accepted May 2006